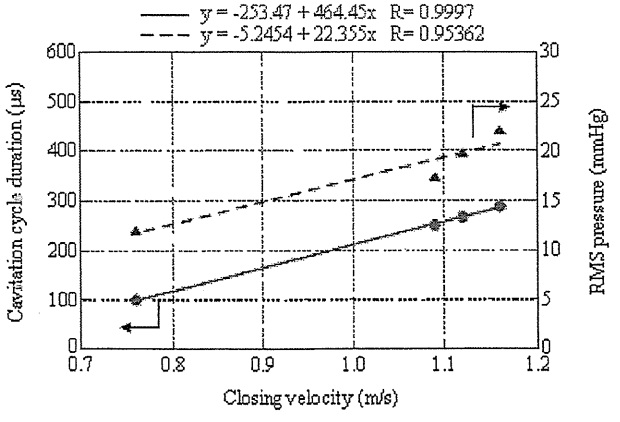

FIG. 10. Relationship between the valve-closing velocity and the cavitation cycle duration and RMS pressure.

compliance structure, so that the peak value of the ventricular pressure reached about 200 mm Hg (Fig. 3). Moreover, higher ventricular pressure occurred, resulting in an extremely high *dP/dt* ranging from 1800 to 2700 mm Hg/s (22). Even with large deviations from beat to beat, the driving pressure slope has a tendency to linearly increase with increases in the valve-closing velocity (22). In the present study, the cavitation cycle duration and the RMS pressure increased as the valve-closing velocity increased linearly (Fig. 10). This indicates that the valve-closing velocity was valid for estimating the MHV cavitation intensity in our PVAD.

In a previous study, we reported that the inlet valve orientation angle of the monoleaflet valve in our PVAD affected the flow pattern inside the pump (18). In the future, we will investigate the orientation angle of the inlet valve effect on the cavitation intensity using the monoleaflet valve. Moreover, most of the MHVs currently in clinical use are bileaflet valves. It is possible that monoleaflet valves will become unavailable in the future. Therefore, we will also be investigating the washout effect inside the PVAD with a bileaflet valve.

CONCLUSIONS

We attempted to synchronize cavitation images and acoustic signals of cavitation bubbles using a PVAD. The cavitation was concentrated at the valve stop, and the major cause was squeeze flow. At a low valve-closing velocity, bubble cavitation was observed near the valve stop, while at a fast valve-closing velocity, cloud cavitation was observed. The valve-closing velocity was related linearly to the cavitation cycle duration and the RMS pressure. Both the cavitation cycle duration and the RMS pressure are very important factors when estimating MHV cavitation intensity in an artificial heart.

Acknowledgment: This work was supported by the Program for the Promotion of Fundamental Studies in Health Science of the National Institute of Biomedical Innovation.

REFERENCES

1. Knapp RT, Daily JW, Hammitt FG. *Cavitation*. Iowa City, IA: Institute of Hydraulic Research, University of Iowa, 1979.
2. Brennen CE. *Cavitation and Bubble Dynamics*. New York: Oxford University Press, 1995.
3. Kornberg A, Wildhirt SM, Schulze C, Kreuzer E. Leaflet escape in Omnicarbon monoleaflet valve. *Eur J Cardiothorac Surg* 1999;15:867–9.
4. Klepetko W, Moritz A, Mlczoch J, Schurawitzki H, Domanig E, Wolner E. Leaflet fracture in Edward-Duromedics bileaflet valves. *J Thorac Cardiovasc Surg* 1989;97:90–4.
5. Lee HS, Tsukiya T, Homma A, et al. Observation of cavitation bubbles in monoleaflet mechanical heart valves. *J Artif Organs* 2004;7:121–7.
6. Lee HS, Taenaka Y, Kitamura S. Estimation of mechanical heart valve cavitation in an electro-hydraulic total artificial heart. *Artif Organs* 2006;30:16–23.
7. Lee HS, Tatsumi E, Homma A, Tsukiya T, Taenaka Y. Mechanism for cavitation of monoleaflet and bileaflet valves in an artificial heart. *J Artif Organs* 2006;9:154–60.
8. Kleine P, Perthel M, Hasenkam JM, Nygaad H, Hansen SB, Laas J. High-intensity signals (HITS) as a parameter for optimum orientation of mechanical aortic valves. *Thorac Cardiov Surg* 2000;48:360–3.
9. Potthast K, Erdönmen GSchnelke C, et al. Origin and appearance of HITS induced by prosthetic heart valves: an in vitro study. *Int J Artif Organs* 2000;23:441–5.
10. Wu C, Liu JS, Hwang NHC, Lin YKM. Statistical correlation between transient pressure drop and cavitation at closure of a mechanical heart valve. *ASAIO J* 2005;51:11–6.
11. Lukic B, Zapanta CM, Griffith KAWeiss WJ. Effect of the diastolic and systolic duration on valve cavitation in a pediatric pulsatile ventricular assist device. *ASAIO J* 2005;51:546–50.
12. Biancucci BA, Deutsch S, Geselowitz DB, Tarbell JM. In vitro studies of gas bubble formation by mechanical heart valves. *J Heart Valve Dis* 1999;8:186–96.
13. Wu C, Herman BA, Retta SM, Grossman LW, Liu JS, Hwang NHC. On the closing sounds of a mechanical heart valve. *Annal of Biomedical Engineering* 2005;33:743–50.
14. Sneckenberger DS, Stinebring DR, Deutsch S, et al. Mitral heart valve cavitation in an artificial heart environment. *J Heart Valve Dis* 1996;5:216–27.
15. Garrison LA, Lamson TC, Deutsch S, Geselowitz DB, Gaumond RP, Tarbell JM. An in-vitro investigation of prosthetic heart valve cavitation in blood. *J Heart Valve Dis* 1994;3:S8–S24.
16. Sohn K, Manning KB, Fontaine AA, Tarbell JM, Deutsch S. Acoustic and visual characteristic of cavitation induced by mechanical heart valves. *J Heart Valve Dis* 2005;14:551–8.
17. Butchart EG, Li HH, Payne N, Buchan K, Grunkemerier GL. Twenty years' experience with the Medtronic Hall valve. *J Thorac Cardiovasc Surg* 2001;121:1090–100.
18. Akagawa E, Lee HS, Tatsumi EHomma Akihiko, et al. Effects of mechanical valve orifice direction on flow pattern in a ventricular assist device. *J Artif Organs* 2007;10:85–91.
19. Zapanta CM, Stinebring DR, Deutsch S, Geselowitz DBTarbell JM. A comparison of the cavitation potential of prosthetic heart valves based on valve closing dynamics. *J Heart Valve Dis* 1998;7:655–67.

20. Herman BA, Carey RF. A protocol for the evaluation of the cavitation potential of mechanical heart valves. *J Heart Valve Dis* 1994;3:S128–32.
21. Carey RF, Porter JM, Richard G et al. An interlaboratory comparison of the FDA protocol for the evaluation of cavitation potential of mechanical heart valves. *J Heart Valve Dis* 1995;4:532–41.
22. Lee HS, Akagawa E, Homma A, Tsukiya T, Tatsumi E, Taenaka Y. Estimation on mechanical heart valve cavitation in a pneumatic ventricular assist device. *J Artif Organs* 2007; 10:181–5.

Journal of Photopolymer Science and Technology
Volume 21, Number 2 (2008) 225–230 ©2008 CPST

Surface Engineering by Plasma Techniques of DLC for Medical Materials and B lood-compatibility Evaluation

Tatsuyuki Nakatani , Keishi Okamoto , Yuki Nitta, Akira Mochizuki*, Hideo Hoshi and Akihiko Homma****

Toyo Advanced Technologies Co., Ltd.
5-3-38 Ujina-higashi Minami-ku Hiroshima 734-8501, Japan
**Department, of Bio-Medical engineering, Tokai University,*
317 Nishino Numazu Shizuoka 410-0395, Japan
***National Cardiovascular Center*
5-7-1 Fujishiro-dai, Suita, Osaka 565-8565, Japan

The metallic medical devices has high shape stability and durability, but the effects of chemical changes in surface by ingredients inside the body are not negligible. Therefore, metallic medical devices are given surface treatment with carbonaceous thin films or the like. Accordingly, with the purpose of improving the biocompatibility of Diamond-like carbon (DLC) films, we experimented with fabricating biomimetic multifunctional DLC films whose zeta potential is controlled. As a result, we discovered that reducing the Si content is effective for introduction of functional groups onto DLC films. We also succeeded in controlling the zeta potential on DLC surface, by controlling the amounts of anionic and cationic groups introduced. In addition, in assessing the blood compatibility, we found that the DLC surface's zeta potential correlates with the platelet adhesion characteristic and the blood coagulation characteristic; we thus discovered a possibility for optimizing DLC surface engineering. This indicated the possibility that biomimetic materials, multifunctional DLC films using plasma surface treatment techniques could be applied to develop stents and artificial organs with higher biocompatibility.

Keywords: Diamond-Like-Carbon, silicon, plasma treatment, medical devices

1. Introduction

Amorphous carbon coatings have various advantageous characteristics, such as being deposited at low temperature using plasma enhanced chemical vapor deposition (PECVD), being mechanically and chemically stable, and being superior frictional characteristics. Their industrial application has therefore been advancing at a rapid rate [1,2]. For the future, the emphasis of carbon coating application looks set to shift toward finer materials such as electronic materials and biomaterials. DLC films form extremely smooth, flat, inert surfaces, and much is expected of them as a surface treatment for medical-application materials, where interaction with biological matter is to be avoided [3-9]. For these reasons, greater control over structure and surface functionalization is likely to become important in thin film fabrication.

We have previously reported on the application of DLC films to drug-eluting stents for coronary arteries [10,11]. As Fig. 1 shows, coronary artery stents take the form of a metallic mesh tube. They are medical devices that are used for treatment of symptoms arising from stenosis or occlusion of coronary arteries, and secure the flow of blood by being left in place after insertion to the disease part. Our DLC films for stents was developed as a highly–tenacity, Si concentration gradient-type DLC films that is able to track deformation of the

Received April 7, 2008
Accepted May 16, 2008

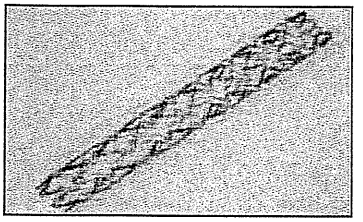

Fig. 1 Photograph of coronary artery stent (diameter ≈ 3.0mm, length ≈ 15mm)

base material and does not have cracks [10]. Further, the surface modification method that we developed employs introduction of functional groups by plasma irradiation onto the DLC films. Specifically this is a method whereby firstly, reactive sites of carbon radicals or the like are formed on the DLC films through plasma irradiation, then the surface is exposed to the atmosphere so as to generate functional groups such as hydroxyl groups, which are then used as footholds for coating with drug-containing biodegradable polymer.

However, as the drug-containing biodegradable polymer is designed to elute into the blood for several weeks after being left inside a artery, the DLC surface will ultimately come into contact with endothelial cells or blood. Also, non-coated stents, which do not use drugs or biomolecules, have been increasingly under review in recent years. Therefore, imparting biocompatibility on DLC films ranks as an important task in order to functionalize the surfaces of stents and artificial organs.

Accordingly, we have studied the possibility of imparting biocompatibility by controlling the functional groups that are generated on the surface of DLC films using plasma surface treatment techniques. We believe that thereby the creation of a new DLC films that is both durable and functional can be expected. We are focusing particularly on interaction between the DLC surface and biomatter. Cells are held to generally be negatively charged, and the zeta potential of their surfaces varies with each cell. Hence it is surmised that it will be possible to control interaction with DLC surface and cells that wishes to cause to adhere by having same zeta potential or be not adsorbed. Therefore, controlling zeta potential is an important requirement for achieving a DLC surface that is inert with regard to cells. The zeta potential control method that we focused on was introduction of anionic groups and cationic groups by using plasma surface treatment. Fig. 2 is a schematic of a DLC surface with functional groups introduced. Anions are negatively charged ions, and cations are positively charged ions. Hence, if the ratio of composition of these functional groups that are introduced can be controlled at the DLC surface, it should be possible to control the zeta potential and thus to have particular cells selectively adhere or be not adsorbed by the DLC surface.

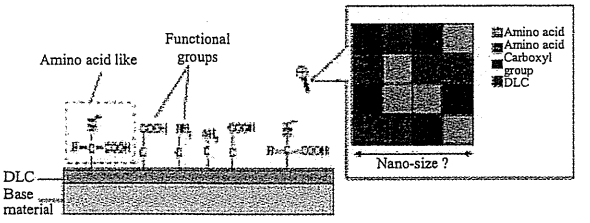

Fig. 2 Schematic of DLC surface with functional groups introduced

In this study, we attempted plasma surface treatment on DLC films so as to experiment with introduction of functional groups to its surface. We also measured the zeta potential of DLC film with anionic groups and cationic groups introduced. Further, by introducing anionic groups and cationic groups simultaneously on a DLC surface, we created a biomimetic DLC films with zwitterions structure. And then, we investigated the relation between zeta potential and blood compatibility by various conditions on the DLC films.

2. Experimental method

2.1. Preparation of DLC thin film

To investigate,10 mm square, 1 mm thick pieces of cobalt chrome (CoCr) alloy were used as the samples. An ionized deposition apparatus was used for deposition the DLC films. Plasma was generated by introducing argon (Ar) and benzene (C_6H_6) gases serving as the ion sources into a plasma generation source that used thermions obtained from a filament installed inside a process chamber.

First of all, the samples was placed inside the chamber of the ionized deposition apparatus, and Ar gas was introduced in so as to render the pressure 10^{-1} to 10^{-3} Pa. Then bombardment cleaning was implemented for about 30 minutes by discharge.

Following that, tetramethylsilane ($Si(CH_3)_4$) and C_6H_6 were passed in, adjusting the deposition pressure 10^{-1} Pa. While introducing gas in continuously at a rate of 30 ml/min, C_6H_6 gas was ionized and a DLC films was deposited. An amorphous DLC film, with a thickness 30 nm and mainly consisting of silicon (Si), carbon (C) and hydrogen (H), was deposited on the surface of the sample. DC bias voltage was -1.5kV. Also, the temperature of the substrate during the thin film deposition was about 160°C.

2.2. Plasma surface treatment

There follows a description of the plasma surface treatment apparatus. The chamber interior was evacuated to below 5 Pa with a rotary pump, the pressure being measured with a Pirani gauge. The process chamber was connected to an RF power source with maximum output 300 W (Adtec Plasma Technology, model AX-300; frequency 13.56 MHz), and RF electric power of 30 W was injected as the plasma generating power. Capacitively-coupled plasmas was generated by means of two parallel plate electrodes. The operation gases were oxygen, Ar and ammonia (NH_3), which were introduced into the chamber by a mass flow controller. The duration of plasma irradiation was 15 seconds, or 30 seconds for continuous treatment with the gas varied.

2.3. Surface analysis

The functional groups introduced on the surface of the DLC films were analyzed by using X-ray photoelectron spectroscopy (XPS). The instrument used for this was a JEOL JPS9010 XPS apparatus. Non-monochromatized AlK α rays (1286.3 eV) were used as the X-ray source, with the accelerating voltage set at 12.5 kV and the emission current at 15 mA. The measurements were made at room temperature, under pressure of 8.0×10^{-7} Pa. The main peaks of the C1s spectra obtained were corrected by adjustment to the binding energy of amorphous carbon, 284.3 eV [12], and the backgrounds were eliminated using the Shirley method [13]. The measurements focused on the carboxyl groups. To measure the carboxyl groups, peak splitting was carried out by taking peaks on the 4.3eV high coupling energy side of the C1s peak as being O=C-O bonds. Further, the C1s peaks were split by assuming 287.1 eV for the C=O bonds and 285.8 eV for the C-O bonds [14]. To cross-check that the surface of the DLC film had been modified with functional groups, we measured the surface's zeta potential and assessed the correlation with the XPS analysis results. An Otsuka Electronics ELS-Z was used to measure the zeta potential. The measurement method was as follows. Plasma-irradiated DLC films was attached to a chamber for plate sample, and the chamber interior was filled with monitoring particles dispersed in purified water. Electrophoresis of the monitoring particles was implemented for each depthwise level of the chamber, and the apparent velocity distribution in the chamber interior was determined. The conditions for implementation of electrophoresis were 17.33 V/cm average field, 1.02 mA average current. The zeta potential of the DLC films surface was derived by using the Mori-Okamoto equation [15] to analyze the apparent velocity distribution obtained.

2.4. Evaluation of blood compatibility

To assess blood compatibility, we assessed two items: platelet adhesion characteristic and blood coagulation characteristic. Fig. 3 is a schematic diagram of the process of assessing the thrombin-antithrombin III complexes (TAT) production quantity. To determine the blood coagulation characteristics, heparinized whole blood (1,000 μl) was pipetted into a chamber with 2,613 mm^2 of surface area (40-mm diameter) and the chamber was rotated vertically at 47 rpm at 37 °C for 120 minutes to avoid sedimentation of blood cells during incubation. After incubation, the blood was moved to a micro-test-tube, followed by addition of 10% sodium citrate solution. The blood was centrifuged at 3,000 rpm for 10 min to obtain

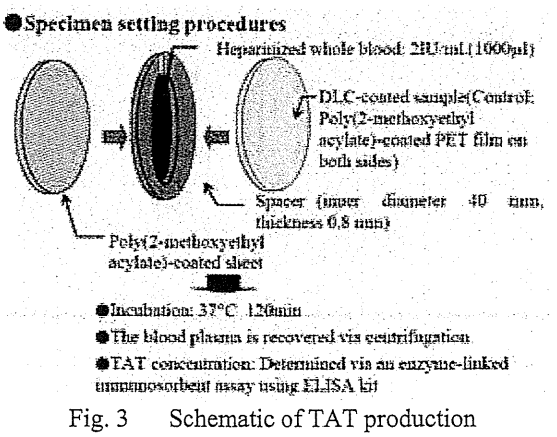

Fig. 3 Schematic of TAT production quantity assessment

plasma. The level of TAT in the blood plasma was evaluated using an ELISA kit (TAT-EIA, Enzyme Research Laboratories) and microplate reader (Thermo Max, Molecular Device Corporation). The amount of platelets adhering to the samples was measured in the following manner. 130 μl of blood plasma (1×10^5 platelets/μl) was placed on the poly(2-methoxyethyl acylate)-coated PET film and incubated for 60 minutes at 37 °C. After the film was washed, it was immersed in 1% glutaraldehyde in phosphate-buffered saline (PBS) for 60 minutes at 4 °C to fix the adherent platelets. The sample was freeze-dried and sputter-coated using platinum, prior to observation by scanning electron microscopy (JSM-840, JEOL).

3. Results and discussion

3.1. Control of introduction of functional groups to DLC surface

We studied efficient introduction of functional groups to the DLC surface. For the measurements, we used an angle-resolved XPS analysis method [16]. Using this method, we first analyzed the composition of Si-doped DLC, then used Ar and O_2 plasmas to form functional groups on the DLC surface and assessed the correlation with the amount of doped Si. First, the O=C-O bonds were determined from C1s spectrum for DLC coated sample having different Si contents. Also, SiC and Si-O were determined from Si2p spectrum.

From the results, the O=C-O bonds were observed to decrease as the Si contents increased. The ratio of intensity of the O=C-O bonds relative to the carbon at such times were: Si (0%) = 5.4%, Si (3%) = 5.0%, Si (19%) = 4.0%, and Si (28.5%) = 1.9% (Fig. 4).

Also, comparison of SiO_2/Si in the DLC having different Si contents gave the composition ratio Si (3%) = 0.64, Si (19%) = 0.55, and Si (28.5%) = 0.48. Thus, it was found that the SiO_2/Si composition ratio did not vary greatly with the Si content. Furthermore, the surfaces were measured and assessed with greater sensitivity by using angle-resolved XPS analysis and varying the incidence angle, specifically by making the X-rays incident at 0°, which is perpendicular to the sample surface, and at the slanted angles 37.5° and 75° (Fig. 5). It can be seen from that figure that as the incidence angle increases, the C1s spectrum decrease and the Si oxides increase. This is probably because O_2 radicals contributed greatly to oxidation of the Si. It could also be explained that oxidation of the Si were easier than carbon, because the electro negativity of Si is 1.9 whereas that of carbon is 2.55.

From the above results, it was evident that in surface treatment using oxygen plasma, the introduction of functional groups via oxidation of carbon in the DLC surface was influenced by the concentration of Si in the DLC surface.

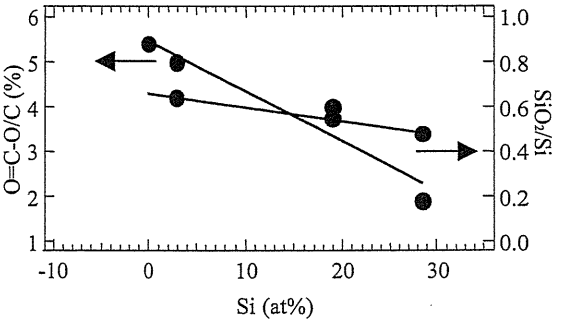

Fig. 4 XPS analysis of C1s and $Si2_P$ spectra of Si-DLC with differing Si concentrations after plasma irradiation

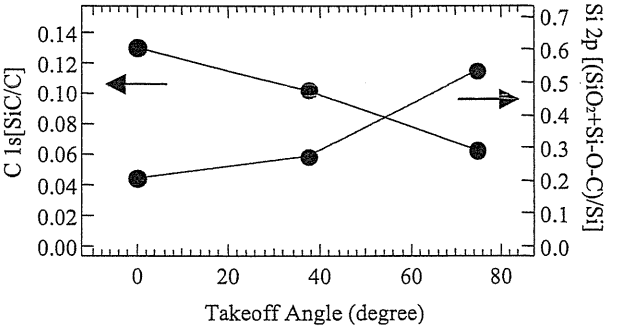

Fig. 5 XPS analysis of C1s and $Si2_P$ spectra of 28.5%-Si-DLC using X-ray incidence angle-resolved

3.2. Zeta potential control of DLC surface

Fig. 6 shows the C1s waveforms were observed when the sample was treated by O_2 plasma. The C1s peaks have been separated into four: C-C, C-O, C=O and O-C=O. Table 1 shows the ratios of O=C-O and N in C1s that were obtains as a results of implementing the plasma surface treatment. These results show that by selecting the gas type it was possible to control the ratio of N to C1s in a range from 0.004 up to 0.052, and to control the ratio of O=C-O to C1s in a range from 0.010 up to 0.052. From these facts it is evident that the C-C bonds or C-H bonds of the DLC surface are braked

by radicals, electrons or ions in the plasma, so that oxidizing reactions such as C-O, C=O, O=C-O, or nitriding reactions, are promoted.

Furthermore, when NH_3 plasma treatment was implemented, peaks originating from nitrogen were found in the XPS measurements. These nitrogen peaks appeared in the neighborhood of 400 eV, which coincides with amino group peaks, which are present at 400±1 eV. It is therefore probable that amino groups were generated on the surface of the DLC films.

Next, we assessed the correlation with the zeta potential. Fig. 7 shows the correlative relationship between the N/O=C-O ratio and the zeta potential. This verified that the larger the N/O=C-O ratio, the greater the zeta potential was, and hence that there was a correlation with the amounts obtained by XPS for the two functional group types. In other words, it was found that the DLC surface was modified by both anionic and cationic functional groups. This would indicate that an zwitterion structure was obtained in the DLC surface. It was also found that the zeta potential was negative with an untreated DLC film, but became positive when the N/O=C-O ratio became large. Where carboxyl groups (-COOH) were present, they generally split as follows:

$$-COOH \rightarrow -COO^- + H^+ \quad [1]$$

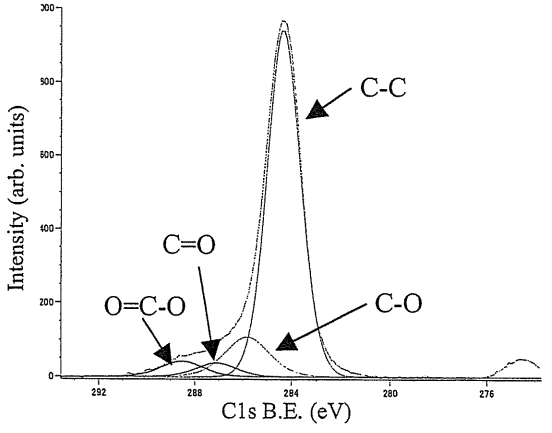

Fig. 6 XPS spectra of DLC surface in C1s binding energy region after O_2 plasma irradiation

Table 1 Plasma treatment gases, and functional group ratio obtained therewith

First gas	O_2	Ar	NH_3	Ar	O_2	DLC
Second Gas	-	-	-	NH_3	NH_3	-
[N]/[C]	0.004	0.006	0.126	0.043	0.146	0.004
[COO]/[C]	0.048	0.052	0.010	0.033	0.010	0.017
[N]/[COO]	0.08	0.11	12.48	1.31	15.01	0.26

and the sample became negatively charged. This was probably the cause of the zeta potential declining as the -COOH increased. Also, the fact that the zeta potential became positive was probably due to the influence of amino groups ($-NH_3^+$) in which protons had bonded. The present experiments did not examine the influence of hydroxyl groups and carbonyl groups on the zeta potential; this will need to be studied in the future. Such study will need to include elucidation of domain formation.

The foregoing results demonstrate that the surface potential can be controlled by the ratio of composition of carboxyl and amino groups that are introduced, which indicates a possibility of imparting tissue cell compatibility to the DLC films.

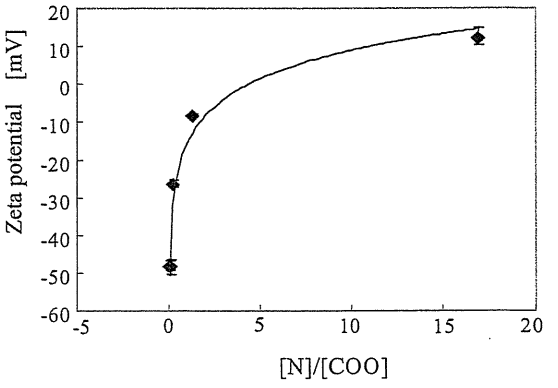

Fig. 7 [N]/[COO] ratio versus zeta potential

3.3. Fabrication of biomimetic DLC and evaluation of blood compatibility

Fig. 8 shows the relation between the ratio of the N component to the O=C-O component on the one hand, and compatibility with regard to the amounts of TAT produced and amounts of platelets adhering, on the other. The N component to O=C-O component ratio N/O=C-O in the figure was derived using (N/C)/(O=C-O/C). As this figure shows, the greater the N/O=C-O ratio, the higher the compatibility with regard to the blood coagulating factors. Thus, it was found that optimal compositional ratio also exist in an zwitterion structure, resulting in the film showing superior blood compatibility if the zeta potential is high. However, it is not clear why the film exhibits superior compatibility with regard to both platelets adhesion and blood coagulating factors when the O=C-O/C component ratio is low and the N/C is

high. But O=C-O/C is a functional group possessing a negative charge, while N/C is a functional group possessing a positive charge. Thus, it might be that influence to blood-compatibility is exerted by the amounts of the positive and negative charges, and by the distances between the functional groups, on the surface of the carbonaceous films.

The foregoing results indicate that by optimizing the amounts of carboxyl and amino groups introduced to the DLC surface we have succeeded in developing an zwitterion structure. This biomimetic DLC film may be suggested as a new biocompatible material with high blood compatibility compared to conventional DLC.

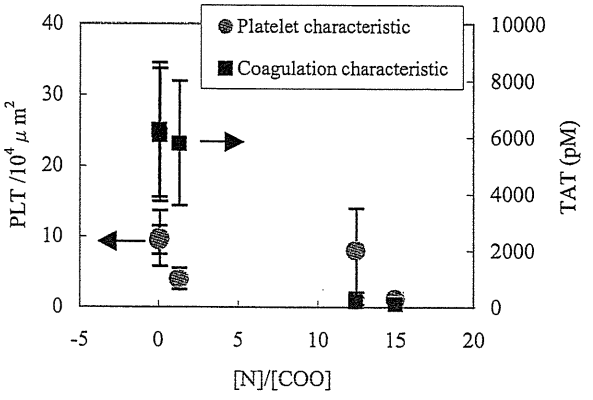

Fig. 8 Relation between [N]/[COO] ratio and blood coagulation and platelet adhesion characteristics

4. Conclusion

We established that reducing the Si content is effective for introduction of carboxyl and other functional groups to DLC surface. We also found that the amounts of anionic and cationic groups introduced can be controlled by altering the plasma irradiation conditions. Further, we succeeded in obtaining zeta potentials spread over a wide range by varying the amounts of functional groups introduced to the DLC surface. In addition, we found that by optimizing the amounts of carboxyl and amino groups introduced to the DLC surface, its blood compatibility is enhanced compared to untreated DLC. Through the experiments, we discovered that there is a possibility that multifunctional DLC film using plasma surface treatment technique can be used on the surfaces of coronary artery stents, and other equipment.

Acknowledgements

We wish to thank Dr. Shuzou Yamashita of Japan Stent Technology, the promoter of the joint project on stents, for his multifaceted assistance to us in carrying out our research. We also acknowledge gratefully the kind advice we received on plasma techniques from Emeritus Professor Noriyoshi Sato of Tohoku University, on film surface evaluation methods from Professor Takayuki Takahagi of Hiroshima University.

References

1. T. Nakatani, K. Okamoto, A. Araki, T. Washimi, New Diamond and Frontier Carbon Technology, **16** (2006) 187.
2. C. Weissmantel, K. Bewilogua, K. Breuer, D. Dietrich, U. Ebersbach, H. J. Erler, B. Rau and G. Reisse, Thin Solid Films, **96** (1996) 31.
3. D. P. Maguire, Diamond and Related materials, **14** (2005) 1277.
4. B. Balram, et al., Catheterization and Cardiovascular Interventions, **67** (2006) 698.
5. T. Hasebe, A. Kamijo, A. Hotta, K. Takahashi, T. Suzuki, Chemistry and Chemical Industry, **59** (2006) 1064.
6. R. Hauert, Tribology International, **37** (2004) 991.
7. R. Hauert, Diam. Relat. Mater., **12** (2003) 583.
8. M. I. Jones, I. R. McColl, D. M. Grant, K. G. Parker, T. L. Parkar, *J.* Biomed. Mater. Res., **52** (2000) 413.
9. D. Antoniucci, et al., Am. J. Cardiol., **85** (2000) 821.
10. T. Nakatani, K. Okamoto, I. Omura, S. Yamashita, J. Photopolym. Sci. Technol., **20** (2007) 221.
11. K. Okamoto, T. Nakatani, S. Yamashita, S. Takabayashi, T. Takahagi , Surface and Coating Technology, **in press.**.
12. Handbook of X-ray Photoelectron Spectroscopy , JEOL, (1991) p.155.
13. A. Jablonsk, Surf. Interface Anal., **23** (1995) 13.
14. J. S. Brinen,, S. Greenhouse, L. Pinatti, Surf.Interface Anal., **17** (1991) 63.
15. H. Mori, H. Okamoto, Fusen, **27** (1980) 117.(in Japanese)
16. S. Takabatashi, K. Motomitsu, T. Takahagi, A. Terayama, K. Okamoto and T, Nakatani, J. Appl. phys., **101** (2007) 103542.

Photoinduced Cross-Linking of Star Vector for Improvement of Gene Transfer Efficiency

Yasushi Nemoto,[†,‡,§] Yue-Min Zhou,[†,||] Eisuke Tatsumi,[||] and Yasuhide Nakayama*[,†,§]

Department of Bioengineering and Department of Artificial Organs, Advanced Medical Engineering Center, National Cardiovascular Center Research Institute, 5-7-1 Fujishiro-dai, Suita, Osaka, Japan, Development Department, Chemical Products Division, Bridgestone Corporation, 1 Kashiocho, Totsuka-ku, Yokohama, Kanagawa, Japan, and Division of Molecular Chemistry, Graduate School of Engineering, Hokkaido University, N13−W8, Kita-ku, Sapporo, Hokkaido, Japan. Received January 5, 2008; Revised Manuscript Received October 2, 2008

This study aimed to investigate the effect of cross-linking of a cationic nonviral gene carrier on gene expression. As a precursor for photo-cross-linking, a star-shaped, six-branched cationic polymer of poly(*N,N*-dimethylaminopropylacrylamide) (six-branched star vector, SV), which was previously designed as a gene carrier, was synthesized by iniferter-based living radical polymerization. Upon UV irradiation, the number-average molecular weight (M_n) of the SV increased from ca. 28 kDa to ca. 32 kDa (irradiation time, 180 min) and ca. 46 kDa (240 min) with broadness of the polydispersity due to the coupling reaction between the polymer radicals generated at the terminal ends of each branch of the SVs, resulting in the preparation of cross-linked SVs (CSVs) without the use of any chemical cross-linking agents. Irrespective of cross-linking, all the SVs were able to interact with and condense luciferase-encoding plasmid DNA to yield relatively stable polymer/DNA complexes (polyplexes) of approximate diameter 150 nm with ζ-potential of ca. 20 mV. However, a transfection study using several types of cell lines, HeLa, Hep G2, 293, and COS-1, showed that by cross-linking of SVs the luciferase activity increased drastically. The activity with CSV (M_n = ca. 46 kDa) was increased by at least 1 order of magnitude in the original SV (M_n = ca. 28 kDa), which was several-fold that in the SV with the same molecular weight in all cells. In all SVs, no significant cellular cytotoxicity was observed even at a high charge ratio of 45. The SV-based gene transfection was significantly enhanced by the cross-linking of the SVs.

INTRODUCTION

Several successful clinical trials reported thus far have involved viral vector systems (such as retroviruses and adenoviruses) that provide efficient transduction and high levels of gene expression (*1*−*3*). However, their severe immunogenicity and toxicity remain major obstacles in viral vector-mediated gene therapy. For these reasons, nonviral vectors have been introduced as an alternative to such hazardous viral vectors, and they are being studied for their potential in providing safer and more desirable methods of gene delivery and clinical gene therapy (*4*−*8*).

Studies have been conducted in many laboratories to improve the gene delivery efficiency of polymeric gene carriers and to reduce their cytotoxicity. In these studies, nanoarchitectural, macromolecular design of the polymeric carriers by hyperbranching or cross-linking has been attempted as one of the major strategies (*9*−*17*). Starburst polyamideamine dendrimers—a relatively new class of highly branched spherical polymers that are strongly soluble in aqueous solution and have a unique surface of primary amino groups—have been established as one of the core structural components of synthetic gene carriers (*9*−*12*). Further, chemical cross-linking techniques have been used by combining preexisting carriers in order to improve gene delivery efficiency or reduce cytotoxicity. (*14*−*16*) For example, an ester or disulfide bond, which can be cleaved with common reducing agents after conjugation, has been utilized for carrier biodegradation. It has recently been established that branched high-molecular-weight polyethyleneimine (PEI) (>25 kDa) is an effective transfection agent, and recent reports indicate that low-molecular-weight PEI (~10 kDa) has relatively lower toxicity (*18*, *19*). Therefore, low-molecular-weight PEI was cross-linked by biodegradable bonding to obtain high gene delivery efficiency and low toxicity (*15*, *16*).

A branching structure was also introduced to improve the functionality of the carriers (*14*). When naturally occurring polymers or synthetic peptides were attached on the side chains of PEI, a high transfection efficiency was obtained (*20*−*22*). However, in case PEI components were used unmodified, the transfection efficiency of the branched form was generally lower than that of the linear form (*23*). On the other hand, we attempted to investigate the usefulness of a series of star-shaped cationic polymers as a base chemical structure for a novel high-performance gene carrier (*24*−*28*). These polymers, known as star vectors (SVs), were prepared by initiator-transfer agent-terminator (iniferter)-based living radical polymerization (*29*, *30*) of *N,N*-dimethylaminopropylacrylamide (DMAPAAm) by using their respective multidithiocarbamate (DC)-derivatized benzenes (multifunctional iniferters). The gene expression efficiency in COS-1 cells improved significantly with an increase in the number of branches and the molecular weight of the SVs (*24*). It was recently shown that attaching each cationic branch in SV with nonionic block chains (*25*) or peptides (*26*) as ligands resulted in a considerable improvement in the gene transfection

* To whom correspondence should be addressed: Department of Bioengineering, Advanced Medical Engineering Center, National Cardiovascular Center Research Institute, 5-7-1 Fujishiro-dai, Suita, Osaka 565-8565, Japan. Telephone: (+81) 6-6833-5012 (ex.2624). Fax: (+81) 6-6872-8090. E-mail: nakayama@ri.ncvc.go.jp.

[†] Department of Bioengineering, National Cardiovascular Center Research Institute.

[‡] Bridgestone Corporation.

[§] Hokkaido University.

[||] Department of Artificial Organs, National Cardiovascular Center Research Institute.

10.1021/bc800003t CCC: $40.75
Published on Web 11/13/2008

efficiency and the targeting of the vector to specific cells such as resting macrophages. Other star-shaped polymers were synthesized by conjugating multiple oligoethyleneimine arms onto an α-cylodextrin core, based on a similar concept used in our molecular design (*31*). These star-shaped polymers, including SVs, are promising new nonviral gene delivery vectors with low cytotoxicity and high gene transfection efficiency that can have gene therapy applications in the future.

The number of branches in SVs enhances the gene expression efficiency as described above (*24*). Therefore, additional complex branching by cross-linking of SVs is expected to further improve gene transfection efficiency. To this end, we synthesized cross-linked SVs (CSVs) by using molecular design wherein we exploited the photoreactive property of DC groups, which theoretically exist at the terminal ends of each branch in SVs after preparation. Further, the effects of the molecular structure and mass of SVs before and after cross-linking on their transfection properties and cytotoxicity were evaluated.

EXPERIMENTAL PROCEDURES

Materials. Chloroform of a special grade was treated with N_2 gas bubbling before use. N_2 gas of G1 grade (Japan Fine Products Co., Kanagawa, Japan) and 99.9999% purity or more was used. Diethyl ether of a special grade was used for polychlorobiphenyl (PCB) analysis; it was stabilized with ethanol and not butylhydroxytoluene (BHT). DMAPAAm purchased from Tokyo Kasei Co. (Tokyo, Japan) was used after distillation (bp 105−110 °C/0.3 mmHg). Other solvents and chemical reagents, all of which were of a special reagent grade, were purchased from Kanto Chemical Co. (Tokyo, Japan) or Aldrich (Milwaukee, WI) and were used without any purification. Purified and DNase-free pyrogen water with a conductance of 18 MΩ or more was prepared using Puric MX-II (Organo Inc., Tokyo, Japan). The 5266-bp pGL3 control vector (Promega Inc., Tokyo, Japan) encoding luciferase was used as luciferase reporter plasmide DNA; it was amplified in competent *Escherichia coli* (Promega Inc.) cells and purified using Maxiprep according to a protocol of QIAGEN (Tokyo, Japan). The purity of the amplified pDNA was assessed by electrophoresis on a 1% agarose gel, and the concentration was determined by UV absorbance at 260 and 280 nm.

Synthesis of 1,2,3,4,5,6-Hexakis(*N,N*-diethyldithiocarbamylmethyl)benzene (Iniferter) (*24, 25*). An ethanol solution (100 mL) of 1,2,3,4,5,6-hexakis(bromomethyl)benzene (1.0 g, 1.6 mmol) and sodium *N,N*-diethyldithiocarbamate trihydrate (6.4 g, 28.2 mmol) was stirred for 96 h at room temperature. The resulting precipitate was filtered, washed three times with approximately 1 L of methanol, and recrystallized using a chloroform/methanol solution. The yield of 1,2,3,4,5,6-hexakis(*N,N*-diethyldithiocarbamylmethyl)benzene was 1.5 g (yield, 90%). ^{1}H NMR (in chloroform-d_1): δ 1.26−1.31 (m, 36H, -CH_2−CH_3), 3.71−3.73 (q, 12H, -N-CH_2-), 3.99−4.01 (q, 12H, -N-CH_2-), 4.57 (s, 12H, Ar-CH_2).

Synthesis of Six-Branched Cationic Polymer (Six-Branched Star Vector, SV) (*24, 25*). 1,2,3,4,5,6-Hexakis(*N,N*-diethyldithiocarbamylmethyl)benzene (45.6 mg, 63 mmol) was dissolved in approximately 20 mL of chloroform. DMAPAAm (7.88 g, 50.5 mmol) was added to the solution. The total volume of the solution with chloroform increased to 50 mL. The concentrations of the iniferter and monomer were 5.0 mM and 1.0 M, respectively. The mixture was poured into a hard-glass cubic cell (4 mm × 40 mm; glass thickness, 3 mm), following which N_2 gas was bubbled into the glass cell at a flow rate of 2 L/min for 10 min to remove the O_2 gas from the solution. The solution was irradiated for 30 min with UV light (light intensity: 2.5 mW/cm^2). The reaction mixture was concentrated to approximately 10 mL by using a rotary evaporator and poured into 1.0 L of diethyl ether to obtain a polymeric precipitate. The diethyl ether solution supernatant was removed by decantation. Reprecipitation was carried out 3 times in a chloroform/diethyl ether system. The final precipitate was dried under vacuum and dissolved in an adequate quantity of H_2O. The resultant aqueous solution was filtered with a disposable syringe filter unit having a pore size of 0.22 um (Mixed Cellulose Ester, Toyo Roshi Ltd., Tokyo, Japan) and freeze−dried for 72 h using a vacuum pump (GCD136X, ULVAC, Tokyo) and freeze−dryer (FUD 2200, EYELA, Tokyo) to yield six-branched poly(D-MAPAAm) powder. The molecular weight was determined by gel permeation chromatography (GPC) analysis: M_n = 28 kDa. ^{1}H NMR (in chloroform-d_1): δ 1.5−1.7 (br, 3H, -C$\underline{H}_2$-CH- and -CH_2-C$\underline{H}_2$-CH_2-), 1.8−2.0 (br, 1H, -C$\underline{H}$-CO), 2.1−2.2 (br, 6H, -N-C$\underline{H}_3$), 2.2−2.4 (br, 2H, -C$\underline{H}_2$-N(CH_3)$_2$), 3.0−3.2 (br, 2H, -NH-C$\underline{H}_2$-), 7.4−7.8 (br, 1H, -NH). In addition, another branched polymer with M_n of 46 kDa was synthesized using a similar procedure by prolonging the irradiation time to 50 min.

Preparation of Cross-linked Star Vector (CSV). Freeze−dried powder of SV (M_n = 28 kDa) was homogenized in a 100-mL hard-glass tube of thickness 2 mm by vigorous stirring on a magnetic stirrer in a closed system. The O_2 gas in the gas phase of the closed system was replaced with N_2 gas. The mist-like SV powder was exposed to UV light for 180 min by using a 300 W Xenon lamp (MAX-301, Asahi Spectra, Tokyo, Japan) under vigorous stirring. The UV light intensity was adjusted to 1.0 mW/cm^2. After light irradiation, the resulting photoirradiated powder was poured into 50 mL of methanol and centrifuged at 10 000 rpm for 5 min at room temperature to remove the insoluble gel-like precipitate that was produced during irradiation. The obtained supernatant was concentrated to approximately 5 mL by using a rotary evaporator and poured into 500 mL of diethyl ether to recover the polymeric precipitate. The diethyl ether solution was removed by decantation. Reprecipitation was carried out 3 times in a chloroform/diethyl ether system. The final polymeric precipitate was dissolved in H_20, filtered with the syringe filter, and freeze−dried to obtain CSV powder. The molecular weight was determined by GPC analysis: M_n = 32 kDa. In addition, another CSV with M_n of 46 kDa was synthesized using a similar procedure by prolonging the irradiation time to 240 min.

General Procedure. The light intensity from a Xenon lam (MAX-301), measured using a photometer (UIT-150 with UVD-405 detector, USHIO, Tokyo), was adjusted to 2.5 mW/cm^2. UV/vis absorption spectra were recorded using a spectrophotometer (UV-1700, Shimadzu, Kyoto). ^{1}H NMR spectra were recorded in chloroform-d_1 with a 300 MHz NMR spectrometer (Varian Gemini-300) using tetramethylsilane (0 ppm) as the internal standard at room temperature. GPC analysis in *N,N*-dimethylformamide with 30 mM lithium bromide was carried out with a high-performance liquid chromatograph system (LC-10Avp, Shimadzu, Kyoto, Japan) and columns (Asahipack GF-710HQ and Asahipack GF-510HQ, Shodex, Tokyo, Japan) that were calibrated for molecular weight with narrow weight distribution poly(ethylene glycol) (PEG) standards.

Preparation of Polyplexes. SVs with or without cross-linking were dissolved in a saline solution at a concentration of 0.79 μg/μL. In a quartz cell (charge ratio 30), 60 μL aliquots of the saline solution were mixed with 90 μL of Tris-HCl buffered saline solution (pH 7.4) containing the pDNA at a concentration of 3.33 × 10^{-2} μg/μL at room temperature. The solutions (total volume, 150 μL; plasmid concentration, 20 μg/mL) were mixed using a pipet in order to obtain polyplexes. The mean diameters of the polyplexes in the solution were determined by cumulant analysis in a multimodal setting by using the DLS apparatus. During the transfection experiments, which were conducted 10 min after complex formation, 25 μL of the complex solutions

were added into each well of the 24 multiwell dishes (the amount of DNA added to a well, 0.5 μg). Since the data of the particle size were reproducible (n = 20, SD < 10%), only the average values have been described.

Biophysical Characterization of Polyplexes. The ζ-potentials and mean diameters of the polyplexes in a saline solution were obtained by employing dynamic light scattering (DLS) on an ELS-8000 system (Otuska Co., Osaka, Japan) equipped with a 10 mW He−Ne laser. The mean diameters were measured at the concentration that was used for transfection at a C/A ratio of 15, and ζ-potentials were measured after dilution with saline solution to 1/10 of the transfection concentration. The mean diameters were determined by cumulant analysis in multimodal setting.

DNase I Protection Assay. The polyplexes prepared from CSV (M_n = ca. 4.6 kDa) and pDNA (0.5 μg) at the C/A ratio of 15 was added with 5 μL (2 unit) of DNase I (Worthington, DPPF grade). After predetermined incubation time (10 min to 24 h) at 42 °C, 50 μL of a stop solution consisting of 4 M ammonium acetate, 20 mM EDTA, and 2 mg/mL glycogen was added, and the reaction mixture was placed on ice. The aliquot of 5.0 μL was electrophoresed for 30 min at 100 V in 1 wt % of agarose gel by 40 mM TAE running buffer. The gel was stained with 0.5 mg/mL ethidium bromide solution for 30 min to visualized the location of plasmid DNA with a Gel Doc 2000 (Bio-Rad Laboratories, Tokyo, Japan).

Cell Lines. COS-1 african green monkey kidney cells, HeLa human cervix carcinoma cells, HepG2 human hepatocellular carcinoma cells, and 293 human kidney transformed cells were purchased from RIKEN CELL BANK (Tsukuba, Japan). COS-1 cells were maintained in DMEM medium (Gibco, Invitrogen Corp., Carlsbad, CA) with 10% fetal calf serum (FCS, Hyclone Laboratories Inc., Logan, UT), HepG2 cells and 293 cells in MEM medium (Gibco) with 10% fetal bovine serum (FBS, Hyclone), and HeLa cells in MEM medium with 10% FCS. All cells were cultured with 200 units/mL penicillin (ICN Biomedicals Inc., Aurora, OH), and 200 mg/mL streptomycin (ICN) in a 5% CO_2 atmosphere at 37 °C.

In Vitro Transfection and Cell Viability Assays. COS-1 cells were seeded at a density of 3 × 10^4 cells/well in a 24-well plate in medium containing 10% FCS and grown to reach 70−80% confluence prior to transfection for 24 h. HepG2 cells and 293 cells (1 × 10^5 cells/well) were seeded in a 12-well plate and grown in the same way. Transfections were performed with 0.5 μg of plasmid DNA (pGL3 as control) in 24-well dishes containing 0.2 mL of OPTI-MEM I (Gibco) for COS-1 cells and 1 μg of plasmid DNA in 12-well dishes containing 0.4 mL of OPTI-MEM I. After 3 h of incubation, the cells were washed once with PBS (−) and cultured in 1 mL for 24-well or 2 mL for 12-well of appropriate medium for an additional 48 h. The medium was removed, and the cells were washed twice with PBS (−), lysed with 0.2 mL for 24-well or 0.4 mL for 12-well of cell lysis buffer (Promega, Madison, WI), and mixed by vortexing. The lysate was centrifuged at 15 000 rpm for 1 min at 4 °C, and 5 μL of the supernatant was analyzed for luciferase activity by using a Luminous CT-9000D (Dia-Iatron, Tokyo, Japan) luminometer. The relative light unit (RLU)/s values were converted into the amount of luciferase (pg) by using a standard luciferase curve, which was obtained by diluting recombinant luciferase (Promega) in lysis buffer. The protein concentrations of the cell lysates were measured by performing a Bio-Rad protein assay (BIO-RAD, Hercules, CA) with bovine serum albumin as a standard. The final amount of luciferase was determined as the amount of expressed luciferase (mole quantity) standardized to the total protein content of the cell lysate. Data represent the mean ± the standard deviation (S.D.) of the mean (n = 5). Statistical analysis was performed using Student's t-test and p < 0.05 (*) was accepted to be significant.

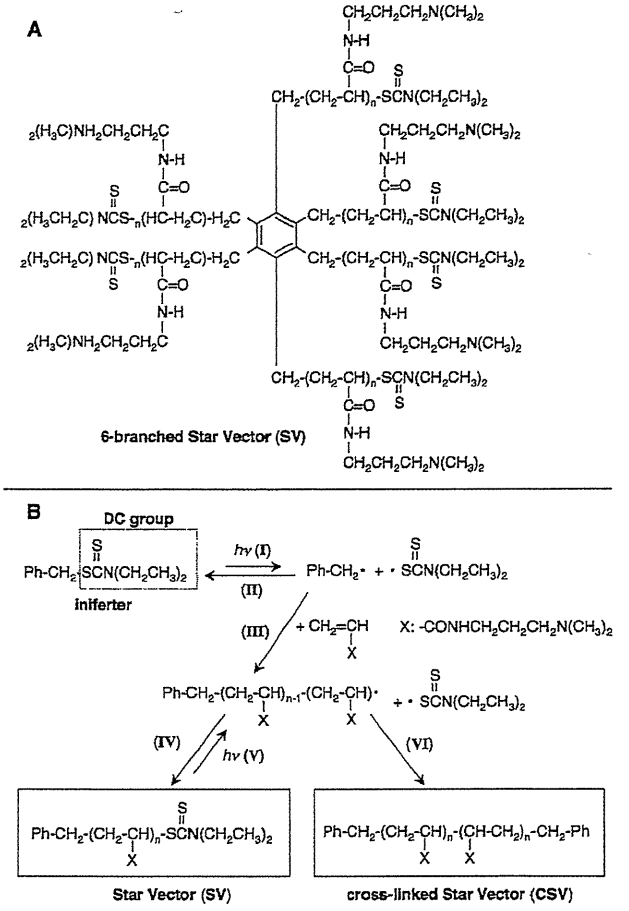

Figure 1. (A) Chemical structure of six-branched star vector (SV). (B) Reaction mechanisms in the preparation of SV through Schemes I, III, and IV from iniferter by photoirradiation in the presence of *N,N*-dimethylaminopropyacrylamide, and those involved in the preparation of cross-linked star vector (CSV) from SVs through Schemes V and VI by photoirradiation under N_2 atmosphere.

Cytotoxicity was assessed by performing a cell viability assay using the WST-8 method (Dojindo, Kumamoto, Japan). The COS-1 cells were seeded 24 h prior to treatment in 96-well plates at 5000 cells/well. The cells were treated under the same conditions as those used for the luciferase assay; 6.2 μL of the transfection mixture containing 0.124 μg of pDNA was added to each well. The cells were treated under the appropriate conditions for 3 h, washed once with PBS, and cultured in 50 μL of DMEM (Gibco) containing 10% fetal calf serum for an additional 24 h. To each well, 10 μL of WST-8 reagent (5 mmol/L) was added. After 2 h of incubation at 37 °C, the absorbance at 450 nm was determined using a Bio-Rad microplate reader (model 680). Data represents the mean ± the standard deviation (S.D.) of the mean (n = 5).

RESULTS AND DISCUSSION

Synthesis and Cross-linking of SV. The two kinds of six-branched SVs with different molecular weights (Figure 1A) were prepared by iniferter-based photoliving radical polymerization via reactions I, III, and IV shown in Figure 1B. The polymerization of a cationic monomer (DMAPAAm) from six-functional inferter, which was synthesized by the derivatization of DC groups to 1,2,3,4,5,6-hexakis(bromomethyl)benzene, was performed by changing the irradiation time. Following 30 min of

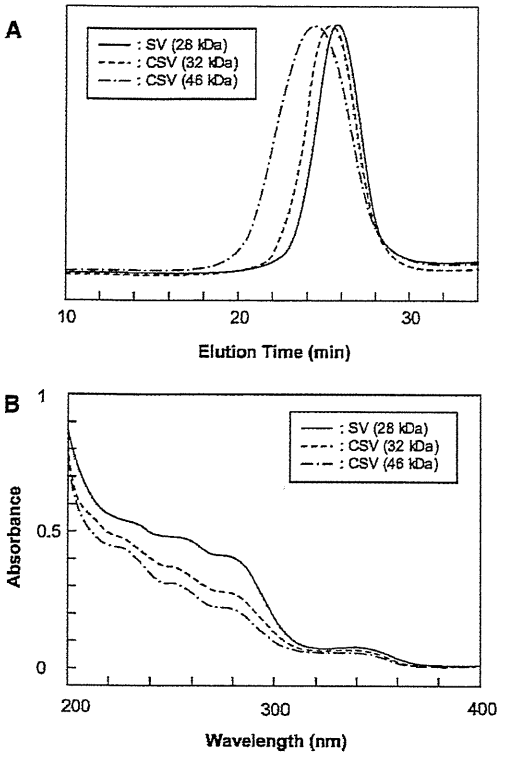

Figure 2. (A) GPC curves and (B) UV absorption spectral changes after photoirradiation of star vectors (SVs) of molecular weight ca. 2.8 kDa to obtain cross-linked star vectors (CSVs) of molecular weight ca. 3.2 kDa (irradiation time, 180 min) and ca. 4.6 kDa (240 min).

UV irradiation, only trace amounts of the SV were observed on GPC, with complete absence of the iniferter (Figure 2A). The obtained SV had a number-average molecular weight (M_n) of ca. 28 kDa with very narrow polydispersity at 1.4 (run 1 in Table 1). By prolonging the irradiation time, the M_n increased to approximately 46 kDa, but the narrow polydispersity (M_w/M_n 1.4) was maintained (run 2).

In the NMR spectrum of the SV with M_n of ca. 28 kDa, after 20 000 cycles, double quartet peaks of two types of *N*-methylene protons appeared at 3.6−3.7 ppm and 3.4−3.5 ppm, indicating the presence of DC groups even after polymerization initiated from the iniferter. On the other hand, the molecular weight of the SV, calculated from the UV spectra (Figure 2B, Table 1), was approximately 32 kDa, which was close to that obtained from GPC measurements (28 kDa). On the basis of these results, we concluded that almost all photoreactive functional DC groups were present at the ω-ends of every branch in the SV.

The mist-like powder of SV with a M_n of ca. 28 kDa was exposed to UV light in a solid phase under a N_2 gas atmosphere in the absence of any monomers. Following 180 min of irradiation, the GPC curve was observed to have shifted slightly to the higher molecular weight side after the gel-like precipitate produced was excluded as a byproduct (Figure 2A). The M_n increased to approximately 32 kDa and the polydispersity broadened (run 1−1 in Table 1). On further increasing the irradiation time to 240 min, a M_n of ca. 46 kDa with an even broader polydispersity was obtained (run 1−2).

Figure 2B shows the UV absorption spectral change of the SVs before and after UV-light irradiation. The specific UV absorption with maximum absorption wavelength at 275 nm originating from the DC group significantly decreased after irradiation. After 240 min of irradiation, the absorption decreased to approximately half the original. The GPC and UV spectral analysis revealed that the SVs were cross-linked by a photoreaction involving the DC groups without the use of any chemical cross-linking agents.

The cross-linking mechanism of the SVs was identified to be as follows. The DC end-capped chain in the SVs finally produced as a precursor was redissociated into a pair of reactive polymer radicals and non- or less-reactive DC radicals by UV irradiation (reaction V in Figure 1B). When there were no monomers in the solid state, simultaneous chain transfer of the generated polymer radicals to the polymer matrix or coupling between the radicals occurred preferentially. Coupling between DC radicals generated *N,N,N′,N′*-tetraethylthiuram disulfide, which is dissociated to dithiocarbamyl radicals by UV irradiation because it is reversible. On the other hand, coupling between polymer radicals generated an SV dimer (reaction VI), which could be not dissociated by UV irradiation. Therefore, the polymer radicals would be selectively consumed by UV irradiation of the SV to generate CSV. As expected, chain transfer of polymer radicals to the polymer matrix also produced CSV in another cross-linking manner, in which the end chains of the SV branch bonded to the side chain of another SV branch. Photoinduced cross-linking with DC groups has previously been performed for the surface modification of medical materials for better biocompatibility (*32*) or polymer design (*33*).

Formation of Polyplexes. Approximately 10 min after mixing a Tris-HCl-buffered solution of pDNA (pGL3-control plasmid) and a saline solution of CSV, the scattering intensity in the DLS measurements was stably observed, indicating that polymer/plasmid complexes (polyplexes) similar to the original SVs had been formed. The effective diameters of the polyplexes prepared from CSV (M_n = ca. 46 kDa), as measured by DLS, were approximately 150 nm at a charge ratio of 15 (Figure 3A). The size was similar to that observed with SVs of almost the same M_n, but it was slightly larger than that with SVs of a low molecular weight (M_n = ca. 28 kDa). All the polyplexes gradually aggregated as incubation proceeded irrespective of whether or not the cross-linking had occurred.

On the other hand, the polyplexes with a higher M_n of ca. 46 kDa were very stable even at a low pH of 4. Up to 180 min after incubation, their small particle size was maintained; however, for the polyplexes from the SV of low M_n (ca. 28 kDa), the particle size increased to approximately 1.5-fold. The particle stability was higher in the polyplexes formed from SVs of a higher molecular weight without any significant dependency on the presence of cross-linking. The moderate ζ-potentials of approximately 20 mV were observed for all particles irrespective of cross-linking and molecular weight (Table 1).

When the polyplexes are formed, it is expected that the digestion of pDNA by DNase I is inhibited. After incubation with DNase I, the polyplexes were analyzed by 1% agarose gel electrophoresis (Figure 4). The pDNA was digested even at 10 min of incubation time. On the other hand, pDNA in the

Table 1. Preparation and Cross-Linking Conditions of SVs and ζ-Potential of the Polyplexes

			UV light irradiation time					
run	[iniferter] (mM)	[monomer] (M)	for polymerization (min)	for cross-linking (min)	M_n (kDa)	M_w/M_n	absorbance at 275 nm	ζ-potential (mV)
1	5.0	1.0	30	-	28	1.4	0.341	17.7 ± 1.0
1−1	-	-	-	180	32	1.7	0.248	16.5 ± 3.3
1−2	-	-	-	240	46	2.0	0.186	18.4 ± 3.9
2	5.0	1.0	50	-	46	1.4	-	15.3 ± 2.4

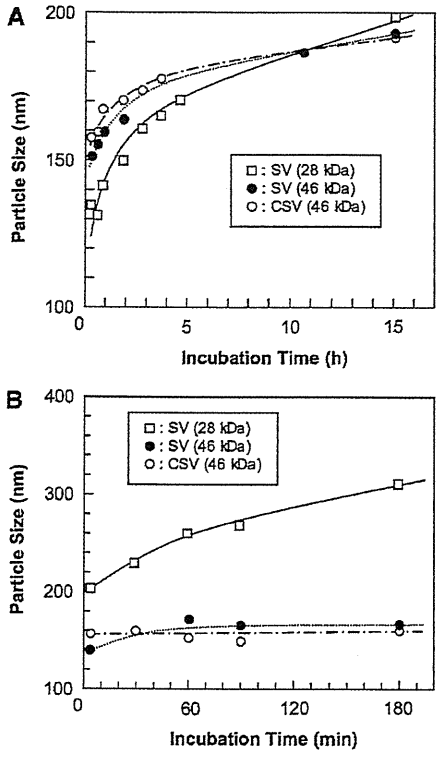

Figure 3. Incubation time-dependent changes in the particle size of polyplexes prepared from luciferase-encoding plasmid DNA nad star vector (SVs) of molecular weight ca. 28 kDa or ca. 46 kDa, or crosslinked star vectors (CSVs) of ca. 46 kDa at pH 7.4 (A) and 4.0 (B). Since the data of the particle size were reproducible (n = 20, S.D. <10%), only the average values have been described.

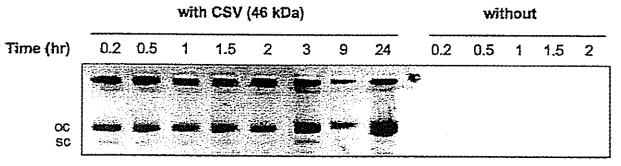

Figure 4. DNase I protection assay. The pDNA with or without CSV at a charge ratio of 15 was treated with DNase I. The position of the open coiled (oc) and supercoiled (sc) forms are indicated on the left.

polyplexes remained even at longer incubation time up to 24 h. The CSV could completely protect the pDNA from digestion of DNase I.

In Vitro Transfection Efficiency. The transfection efficiency of the SVs before and after cross-linking treatment was, at first, tested in the model cell line—COS-1 comprising monkey cells—at a charge ratio of 15 or 30. Since the polyplexes were gradually aggregated as incubation especially in SV with low M_n as indicated in Figure 3, at 10 min after preparation, the polyplexes conducted to the transfection experiments. The cells transfected with the luciferase-encoding plasmid (pGL3) in the absence of any polymer exhibited negligible luciferase expression. In the six-branched SVs, the luciferase expression increased with the molecular weight of the SVs (Figure 5). As shown in Figure 3, the molecular weight dependency may be due to the stability of the polyplexes. A similar dependency was observed for the four-branched SVs, in which a 5-fold increase in molecular weight of the SVs from ca. 10 to 50 kDa induced an approximately 3-fold increase in the luciferase activity. These obtained activities were larger than that in PEI (ExGen 500), which is a major commercially available typical polymeric vector used as a positive control.

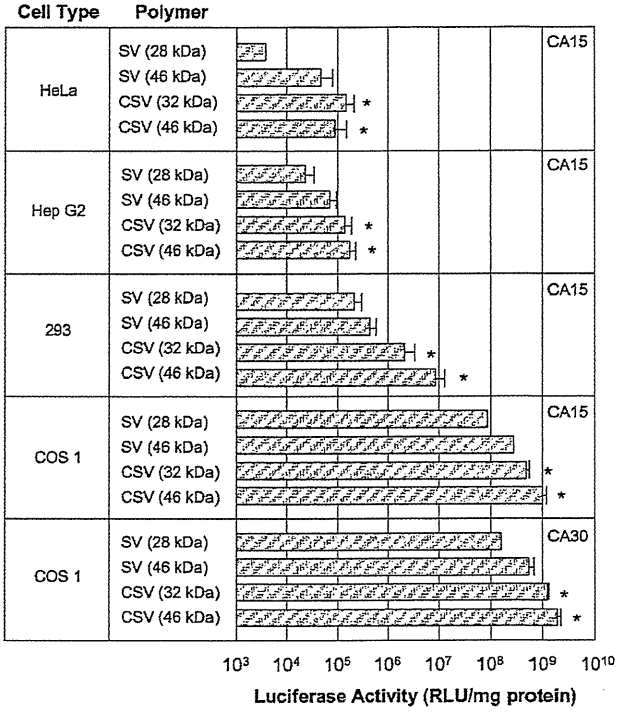

Figure 5. Transfection of four different cell lines using polyplexes prepared by mixing pDNA (pGL3 control, 0.5 μg/24-well plate or 1 μg/12-well plate) and SVs with molecular weight of approximately 28 kDa or 46 kDa, or CSVs with molecular weight of approximately 32 kDa or 46 kDa, at a charge ratio of 15 or 30. For comparison, the transfection efficiency data of polyplexes formed using linear PEI (ExGen 500) at a charge ratio of 5 is also provided. Data represents the mean ± the standard deviation (S.D.) of the mean (n = 5). Statistical analysis was performed using Student's *t*-test and $p < 0.05$ (*) was accepted to be significance.

Interestingly, the transfection activity drastically increased by the cross-linking of the SVs (Figure 5). The activities of CSVs of M_n approximately 32 kDa and 46 kDa at a charge ratio of 15 were approximately 6- and 12-fold the value in the original untreated SV with a M_n of ca. 26 kDa, respectively. For the CSVs with a M_n of ca. 46 kDa, approximately 4-fold higher activity was observed with the cross-linked compound than with the non-cross-linked compound. In addition, an increase in the charge ratio from 15 to 30 induced a further increase in the activity up to approximately 2-fold. Thus, the structural advantage of cross-linking in the SVs was strongly suggested for greater in vitro gene transfection efficiency.

The transfection efficiency was evaluated also in human cell lines—HeLa, human cervix carcinoma cells, HepG2, human hepatocellular carcinoma cells, and 293, human kidney transformed cells. Unfortunately, lower transfection activity was observed in all human cells than that in COS-1 (Figure 5). However, there was a similar drastic increase of transfection activity by cross-linking of SVs. The activity with CSV (M_n = ca. 46 kDa) was at least 1 order of magnitude in the original SV (M_n = ca. 28 kDa). The SV-based gene transfection was significantly enhanced by the cross-linking of the SVs in all cell lines.

Cell Cytotoxicity. The in vitro cytotoxicity of the polyplexes prepared from the regular SVs or photoirradiated SVs was studied as a function of the charge ratio in the range of 5—45 by using the WST assay. As shown Figure 6, in the case of all the polyplexes, the relative cell viability decreased as the charge ratio increased. Polyplexes with a lower charge ratio were considered to have lower cell membrane binding ability, which therefore tended to affect cell viability. In the case of a higher

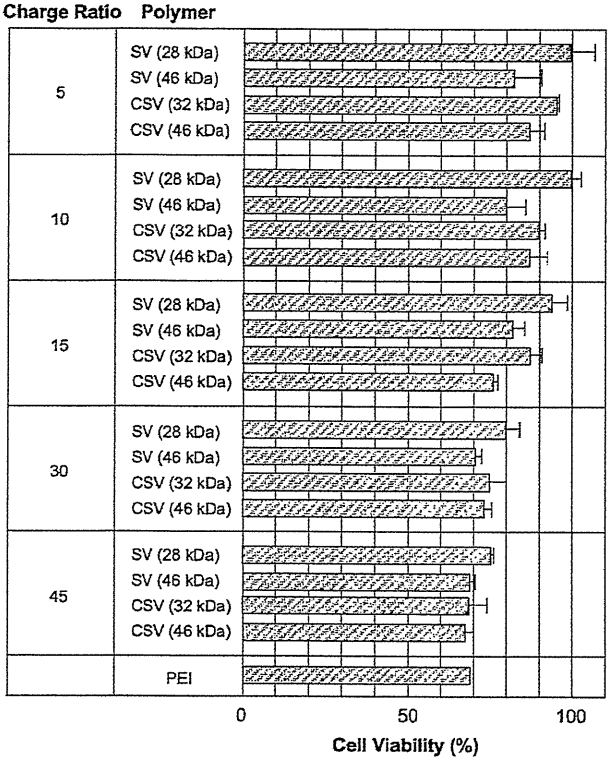

Figure 6. Cytotoxicity of polyplexes prepared by mixing DNA (pGL3 control, 3 μg) and SVs or CSVs at different charge ratios. Cell viability was determined by the WST assay.

charge ratio, it was observed that the polyplexes not only had a higher charge density but also had a higher concentration of the cationic polymer, which was correlated with the cytotoxic effect. Since the molecular weight of the cationic polymer was confirmed as the main parameter affecting its interaction with the cell membrane and, consequently, cell damage, the SVs and photoirradiated SVs of higher molecular weight were considered to have less cytotoxicity at a charge ratio of 30 or 45. However, they might be acceptable, because in these cases, the cell viability was higher than that with polyethyleneimine (PEI) at a charge ratio of 6, and PEI is one of the most popular commercially available gene-delivery agents (Figure 6). There was no significant difference among the polyplexes formed from the SVs and photoirradiated SVs of the same molecular weight. Therefore, it was considered that the photoirradiation treatment of the SVs had no significant disadvantage.

In conclusion, this study successfully demonstrated that SV-based gene transfection was significantly enhanced by the cross-linking of the SVs via any agent except photoirradiation in the solid phase. The M_n of the obtained CSVs increased with increasing irradiation time. With an increase in the M_n of the CSVs, the gene transfection efficiency increased drastically except for HeLa in this study. On cross-linking at charge ratios of both 15 and 30, the transfection activity increased to over 10-fold that of the original SV (M_n = ca. 28 kDa), which in turn was 3-fold that of the SV of the same molecular weight (M_n = ca. 46 kDa). As described in the introduction, nanoarchitectural, macromolecular design of the polymeric DNA carriers by hyperbranching or cross-linking, and so forth, has been attempted as a major strategy for increasing transfection efficiency. Therefore, it was considered that cross-linking of star vector, which could induce an increase in the cationic charge density, would be a key strategy for enhancement of transfection efficiency of cationic polymers. To evaluate the hypothesis, the present study was designed and the effectiveness of the cross-linking of star vector for increasing transfection efficiency was clearly demonstrated. It was considered that the DNA expression using the polyplex was observed by the following five sequential steps: (1) attachment of the polyplexe onto the cell surface, (2) internalization of the polyplexes into the cell, (3) endosomal escape of the polyplex, (4) DNA release from the polyplex, and (5) internalization of DNA into the nucleus. In this study, there were few differences in the ζ-potentials and the mean diameters of all polyplexes, whereas a significant difference was observed in the transfection efficiency between SV and CSV. Therefore, the difference might be greatly induced from the steps after (3).

For further improvement, the CSV-induced gene delivery mechanism should be determined. Although in both SV and CSV excellent colloidal stability with low cytotoxicity was demonstrated, we do not have any additional data to explain the mechanism. In addition, as shown in Figure 2B, a lot of DC groups remained after photo-cross-linking, indicating that the cross-linking only occurred partly. Therefore, it was considered that CSV consisted of a mixture of original SV and cross-linked SV. To purify the CSV, fractionation of the mixture by GPC is ongoing. By using the pure CSV with narrow polydispersity, the mechanism will be explained clearly. Our research in the near future will be directed at optimization of the cross-linking density, macromolecular size and distribution, and combination with other kinds of SVs with different chemical or electrical properties so as to achieve further improvements in the in vitro transfection efficiency for other types of cells and in vivo gene transfection efficiency and in functionalization, including biodegradation ability to obtain low cytotoxicity.

LITERATURE CITED

(1) Mulligan, R. C. (1993) The basic science of gene therapy. *Science 260*, 926–932.
(2) Crystal, R. G. (1995) Transfer of genes to humans: early lessons and obstacles to success. *Science 270*, 404–410.
(3) Kay, M. A., Liu, D., and Hoogerbugge, P. M. (1997) Gene therapy. *Proc. Natl. Acad. Sci. U.S.A. 94*, 12744–12746.
(4) Li, D., and Hung, L. (2000) Gene therapy progress and prospects: non-viral gene therapy by systemic delivery. *Gene Ther. 7*, 31–34.
(5) Luo, D., and Saltzman, W. M. (2000) Enhancement of transfection by physical concentration of DNA at the cell surface. *Nat. Biotechnol. 18*, 33–37.
(6) Gebhart, C., and Kabanov, A. K. (2001) Evaluation of polyplexes as gene transfer agents. *J. Controlled Release 73*, 401–416.
(7) Thomas, M., and Klabanov, A. M. (2003) Non-viral gene therapy: polycation-mediated DNA delivery. *Appl. Microbiol. Biotechnol. 62*, 27–34.
(8) Dubruel, P., and Schacht, E. (2006) Vinyl polymers as non-viral gene delivery carriers: current status and prospects. *Macromol. Biosci. 6*, 789–810.
(9) Kurowska-Latallo, J. F., Bielinska, A. U., Johnson, J., Spindler, R., Tomalia, D. A., and Baker, J. R., Jr. (1996) Efficient transfer of genetic material into mammalian cells using Starburst polyamideamine dendrimers. *Proc. Natl. Acad. Sci. U.S.A. 93*, 4897–4902.
(10) Zhang, X.-Q., Intra, J., and Salem, A. K. (2007) Conjugation of polyamidoamine dendrimers on biodegradable microparticles for nonviral gene delivery. *Bioconjugate Chem. 18*, 2068–2076.
(11) Haensler, J., and Szoka, F. C., Jr. (1993) Polyamidoamine cascade polymers mediate efficient transfection of cells in culture. *Bioconjugate Chem. 4*, 372–379.
(12) Tang, M. X., and Szoka, F. C. (1997) The influence of polymer structure on the interactions of cationic polymers with DNA and morphology of the resulting complexes. *Gene Ther. 4*, 823–832.

(13) Banerjee, P., Reichardt, W., Weissleder, R., and Bogdanov, A., Jr. (2004) Novel hyperbranched dendron for gene transfer in vitro and in vivo. *Bioconjugate Chem. 15*, 960–968.

(14) Kim, T., Seo, H. J., Choi, J. S., Yoon, J. K., Baek, J., Kim, K., and Park, J.-S. (2005) Synethesis of biodegradable cross-linked poly(β-amino ester) for gene delivery and its modification, inducing enhanced transfection efficiency and stepwise degradation. *Bioconjugate Chem. 16*, 1140–1148.

(15) Tomas, M., Ge, Q., Lu, J. J., Chen, J., and Klibanov, A. M. (2005) Cross-linked small polyethylenimines: while still nontoxic, deliver DNA efficiently to mammaliam cells in vitro and in vivo. *Pharm. Res. 22*, 373–380.

(16) Gosselin, M. A., Guo, W., and Lee, R. J. (2001) Efficient gene transfer using reversibly cross-linked low molecular weight polyethylenimine. *Bioconjugate Chem. 12*, 989–994.

(17) Kwok, K. Y., Yang, Y., and Rice, K. G. (2001) Evolution of cross-linked non-viral gene systems. *Curr. Opin. Mol. Ther. 3*, 142–146.

(18) Fischer, D., Bieber, T., Li, Y., Elsasser, H. P., and Kissel, T. (1999) A novel non-viral vector for DNA delivery based on low molecular weight, branched polyethlenimine: effect of molecular weight on transfection efficiency and cytotoxicity. *Pharm. Res. 16*, 1273–1279.

(19) Bieber, T., and Elsasser, H. P. (2001) Preparation of low molecular weight polyethylenimine for efficient cell transfection. *BioTechniques 30*, 74–81.

(20) Wang, Y., Chen, P., and Shen, J. (2006) The development and characterization of a glutathione-sensitive cross-linked polyethylenimine gene vector. *Biomaterials 27*, 5292–5298.

(21) Jiang, H. L., Kim, Y. K., Arote, R., Nah, J. W., Cho, M. H., Choi, Y. J., Akaike, T., and Cho, C. S. (2007) Chitosan-grafte-polyethylenimine as a gene carrier. *J. Controlled Release 117*, 273–280.

(22) Tian, H., Xiong, W., Wei, J., Wang, Y., Chen, X., Jing, X., and Zhu, O. (2007) Gene transfection of hyperbranched PEI grafted by hydrophobic amino acid segment PBLG. *Biomaterials 28*, 2899–2907.

(23) Wightman, L., Kircheis, R., Rossler, V., Carotta, S., Ruzicka, R., Kursa, M., and Wagner, E. (2001) Different behavior of branched and linear polyethylenimine for gene delivery *in vitro* and *in vivo*. *J. Gene Med. 3*, 362–372.

(24) Nakayama, Y., Masuda, T., Nagaishi, M., Hayashi, M., Ohira, M., and Harada-Shiba, M. (2005) High performance gene delivery polymeric vector: nano-structured cationic star polymers (star vector). *Curr. Drug Delivery 2*, 53–57.

(25) Nakayama, Y., Kakei, C., Ishikawa, A., Zhou, Y. M., Nemoto, Y., and Uchida, K. (2007) Synthesis and *in vitro* evaluation of novel star-shaped block copolymers (blocked star vectors) for efficient gene delivery. *Bioconjugate Chem. 18*, 2037–2044.

(26) Mizoguchi, F., Ooe, Y., Hoshino, S., Shimura, m., Kasahara, T., Kano, S., Ohta, T., Takaku, F., Nakayama, Y., and Ishizaka, Y. (2005) Improved gene expression in resting macrophages using an oligopeptide derived from Vpr of human immunodeficiency virus type-1. *Biochem. Biophys. Res. Commun. 338*, 1499–1506.

(27) Zhou, Y. M., Ishikawa, A., Okahashi, R., Uchida, K., Nemoto, Y., and Nakayama, Y. (2007) Deposition transfection technology using a DNA complex with a thermoresponsive cationic star polymer. *J. Controlled Release 123*, 239–246.

(28) Ishikawa, A., Zhou, Y. M., and Nakayama, Y. (2008) Enhancement of star vector-based gene delivery to endothelial cells by addition of RGD-peptide. *Bioconjugate Chem. 19*, 558–561.

(29) Otsu, T., Yoshida, M., and Tazaki, T. (1982) A model for living radical polymerization. *Makromol. Chem. Rapid Commum. 3*, 133–140.

(30) Otsu, T., Matsunaga, T., Doi, T., and Matsumoto, A. (1995) Features of living radical polymerization of vinyl monomers in homogeneous system using N,N-diethyldithiocarbamate derivatives as photoiniferters. *Eur. Polym. J. 31*, 67–78.

(31) Yang, C., Li, H., Goh, S. H., and Li, J. (2007) Cationic star polymers consisting of α-cyclodextrin core and oligoethylenimine arms as nonviral gene delivery vectors. *Biomaterials 28*, 3245–3254.

(32) Nakayama, Y., Takatsuka, M., and Matsuda, T. (1999) Surface hydrogelation using photolysis of dithiocarbamate or xanthate: hydrogelation, surface fixation, and bioactive substance immobilization. *Langmuir 15*, 1667–1672.

(33) Nakayama, Y., Ishikawa, A., Sato, R., Uchida, K., and Kambe, N. (2008) Photodimerization and polymerization of PEG derivatives through radical coupling using photochemistry of dithiocarbamate. *Polym. J.*

BC800003T

J Artif Organs (2008) 11:4–11
DOI 10.1007/s10047-008-0404-9

REVIEW

Journal of Artificial Organs Editorial Committee

Journal of Artificial Organs 2007: the year in review

Key words Artificial heart (basic) · Artificial heart (clinical) · Cardiopulmonary bypass · Artificial lung · Blood vessel prosthesis · Pacemaker · Artificial valve · Biomaterial · Tissue engineering · Dialysis · Apheresis · Artificial liver · Artificial pancreas · Artificial skin · Artificial muscle · Artificial bone · Artificial neuron

Introduction

Members of the Editorial Committee of the *Journal of Artificial Organs* (JAO) are pleased to introduce to colleagues worldwide through the publication of JAO a broad spectrum of important new achievements in the field of artificial organs, ranging from fundamental research to clinical applications. We believe that the JAO has very high potential for promoting interest and research in artificial organs not only in Japan but in other parts of the world, and the specialization, originality, and level of science of the journal are at the highest levels in the field. An electronic version of the JAO has been also available through our publisher's electronic publishing system since 2002. The full text journal is accessible at more than 4000 institutes and libraries in the world. Beginning with Volume 1, papers from Australia, the Czech Republic, Germany, Korea, Poland, Singapore, Sweden, Taiwan, Turkey, the United Kingdom, the United States, and other countries have been accepted for publication, and the cited JAO articles in other journals have also been significantly increasing.

Two years ago we started reviewing and summarizing all the articles published in the JAO in the previous year in order to provide an overview for our readers.[1,2] We have decided to continue this practice this year as well, and we have summarized below the articles published in Volume 10, 2007. Volume 10 of the JAO published 42 articles includ-

Received: February 12, 2008

Y. Sawa (✉)
Division of Cardiovascular Surgery, Department of Surgery, Osaka University Graduate School of Medicine, 2-2 Yamadaoka, Suita, Osaka 565-0871, Japan
Tel. +81-6-6979-3154; Fax +81-3-3879-3159
e-mail: sawa@surg1.medo.osaka-u.ac.jp

E. Tatsumi
Department of Artificial Organs, Advanced Medical Engineering Center, National Cardiovascular Center Research Institute, Suita, Japan

A. Funakubo
Department of Electronic and Computer Engineering, School of Science and Engineering, Tokyo Denki University, Tokyo, Japan

T. Horiuchi
Department of Chemistry for Materials, Faculty of Engineering, Mie University, Tsu, Japan

K. Iwasaki
Waseda Institute for Advanced Study, Waseda University, Tokyo, Japan

A. Kishida
Institute of Biomaterials and Bioengineering, Tokyo Medical and Dental University, Tokyo, Japan

T. Masuzawa
Department of Mechanical Engineering, Ibaraki University, Hitachi, Japan

K. Matsuda
Emergency and Critical Care Medicine, University of Yamanashi Hospital, Chuo, Japan

M. Nishimura
Division of Organ Regeneration Surgery, Tottori University Faculty of Medicine, Yonago, Japan

T. Nishimura
Cardiovascular Surgery, The University of Tokyo Hospital, Tokyo, Japan

Y. Tomizawa
Department of Cardiovascular Surgery, Tokyo Women's Medical University, Tokyo, Japan

T. Yamaoka
Department of Biomedical Engineering, Research Institute, National Cardiovascular Center, Suita, Japan

H. Watanabe
Division of Thoracic and Cardiovascular Surgery, Niigata University Graduate School of Medical and Dental Sciences, Niigata, Japan

ing 25 original papers, 8 review papers, 3 case reports, and 6 brief communications related to the many aspects of the basic research, development, and clinical applications of artificial organs. These included articles on artificial heart, cardiopulmonary bypass, artificial lung, blood vessel prosthesis, artificial valves, dialysis, artificial kidney, biomaterials, tissue engineering, regeneration therapy, regulatory science, and other topics. We are pleased to present such excellent work in our journal. For Volume 10, we had a total of 46 reviewers who are specialists in the field of artificial organs. We offer our profound gratitude to those reviewers for their thoughtful reviews, critiques, and suggestions, which help our authors to improve the work they submit for publication.

Artificial heart (basic)

With regard to basic research on the artificial heart, we published nine articles in total, including two review papers, five original articles, and two brief communications.

E. Tatsumi et al.[3] of the Working Group on the Establishment of Assessment Guidelines for Next-Generation Artificial Heart Systems, Inter-agency Committee for the Guideline Program by the Ministry of Health, Labour and Welfare of Japan and the Ministry of Economy, Trade and Industry of Japan, reviewed the trend in the prevalence of heart failure and examined the potential usefulness of next-generation artificial heart systems in Japan and in other countries. At present, more than 23 million people suffer from heart failure in developed countries, including Japan. Although Japan currently has the lowest mortality from heart failure among those countries, the number of patients is gradually increasing and the associated medical expenses are rapidly growing. The number of heart transplantations, however, is limited due to the overwhelming shortage of donor hearts, not only in Japan but worldwide. Meanwhile, clinical studies and surveys have revealed that the major causes of death in patients undergoing long-term use of artificial heart were infection, thrombosis, and mechanical failure. It is therefore of urgent and universal necessity to develop next-generation artificial hearts that can provide more than 2 years' event-free operation with a superior quality of life and can be used for destination therapy. It is also very important to ensure that an environment that facilitates the development, testing, and approval evaluation processes of next-generation artificial hearts be established as soon as possible.

Y. Abe et al.[4] of the University of Tokyo reviewed the development of mechanical circulatory support devices at their institute. The authors first focused on developing a small total artificial heart (TAH), and the undulation pump was invented to meet this purpose. To date, the authors have implanted the undulation pump TAH (UPTAH) in 71 goats (39–72 kg). They developed and applied a sucking control to prevent atrial sucking, a rapid left–right balance control to prevent acute lung edema, and in addition, 1/R control to stabilize the right atrial pressure. By applying these control methods, seven goats survived more than 1 month, and one goat survived for 63 days. The authors then developed the undulation pump ventricular assist device (UPVAD), which is an implantable ventricular assist device (VAD) based on the technology of the UPTAH. The UPVAD was implanted in six goats, and three goats survived for more than 1 month, indicating its good potential to be an implantable pulsatile VAD.

E. Akagawa et al.[5] of the National Cardiovascular Center of Japan looked into the flow pattern inside a diaphragm-type pneumatic ventricular assist device (PVAD) blood pump, which had been developed in their institute, with respect to the inflow valve-mount orientation. To analyze the flow behavior with different orifice direction (OD) of the valve, the flow pattern in this pump was visualized and analyzed by means of particle image velocimetry. A mono-leaflet mechanical valve was mounted in the inlet and outlet ports of the PVAD, which was connected to a mock circulatory loop tester. As a result, the regional flow velocity was relatively low in the area between the inlet and outlet port roots, and the main circular flow in the blood pump was substantially affected by the OD of the inflow valve. The authors concluded that the OD was an important factor in optimizing the flow condition in their PVAD in terms of preventing flow stagnation.

Two pulsatile motor-driven pumps were reported in 2007. One is a rotating motor-driven pump and the other is a linear motor-driven pump. E. Okamoto et al.[6] of Hokkaido Tokai University have been developing a small, lightweight, motor-driven pulsatile left ventricular assist device with a ball screw. The volume and weight of the device are 285 ml and 360 g, respectively. The blood pump was designed by means of CAD/CAM and computational fluid dynamics (CFD) to optimize blood flow in the pump. An active filling mechanism using permanent magnets was invented, and fuzzy logic position and velocity controller were developed to regulate the pusher plate position precisely. The feasibility of the system was confirmed with in vitro experiments. K. Fukunaga et al.[7] of Kyorin University have developed an implantable direct-electromagnetic left ventricular assist system with a linear oscillatory actuator. The device has a diameter of 100 mm, a thickness of 50 mm, and a weight of 740 g. The full-fill/full-eject driving method with an active filling mechanism which has a sucking release function is applied to drive the pump. An initial animal experiment was performed, and the goat that was the subject of the experiment survived for 42 days with the device. The reason for the termination of the experiment was thrombus formation in the pump. Development of nonpulsatile pumps is the current trend in the field of ventricular assist devices. However, the pulsatile device has good features such as pulsatility, easy-to-estimate flow rate, and preload sensitivity. The development of pulsatile devices remains important and should be supported.

Y. Yamane et al.[8] of the National Institute of Advanced Industrial Science and Technology reported on the hemocompatibility of a nonpulsatile pump with in vitro experiment results. They have been developing a centrifugal pump with hydrodynamic bearings as a long-term implantable

artificial heart. The hemolysis index was reduced by adjusting the pressure distribution around the impeller and expanding the bearing gap. The level of thrombus formation was reduced by changing the groove shapes to increase the bearing-gap flow to 3% of the external flow. The hydrodynamic bearing with lower hemolysis and thrombus formation is a key to the development of a levitation nonpulsatile pump which has no sensing and control modules. The results of this work will contribute to development of better artificial hearts.

The Toyobo–National Cardiovascular Center pneumatic ventricular assist device (Toyobo-NCVC VAD) has been widely used in Japan. However, there has been a serious limitation on mobility of patients because of the large size, heavy weight, and high power consumption of the pneumatic drivers. These issues have been major factors leading to unsatisfactory quality of life for patients. T. Nishinaka et al.[9] from the National Cardiovascular Center and Senko Medical Instrument Manufacturing have developed a compact, low-noise, portable VAD driver by utilizing an electrohydraulic actuator consisting of a brushless DC motor and a regenerative pump. It is compact (33 × 25 × 43 cm) and lightweight (13 kg). This unit can be actuated for as long as 2 h with two rechargeable lightweight batteries as well as with external AC power. The significantly high power consumption of the current VAD pneumatic drivers at more than 400 W is one of the most problematic aspects in transferring patients using any method of transportation. Because a power consumption of less than 50 W was realized in the newly developed Mobart NCVC drivers, these drivers open up new choices of transportation such as ambulances, passenger airplanes, and trains for patients treated with the Toyobo-NCVC ventricular assist devices. Nishinaka et al. conclude that the newly developed portable driver offers the possibility of improving the quality of life and safety of patients supported by pneumatic VADs.

The pneumatic drivers for pulsatile ventricular assist devices allow for the full–empty mode only, whereby the chamber is completely filled and completely emptied in a single pump cycle. Consequently, for the treatment of pediatric patients, the pump rate is the only free parameter to adjust pump flow. In particular, when infants are treated with pneumatic VADs designed for adults, there is no choice but to decrease cardiac frequency unphysiologically low in order to achieve a physiological cardiac output. To overcome these disadvantages, N. Reiss and R. Körfer[10] from the Ruhr University of Bochum have developed a hydraulic drive system. The system can operate in filled–empty mode, by which the chamber is only partially filled in diastole while still being completely emptied in systole. Hence, stroke volume and pump frequency can be set independently in the system. The assist device was applied in eight pigs (weight 9–14 kg) for left ventricular assistance during normal and impaired cardiac function (pacing induced cardiac shock, mean arterial blood pressure less than 40 mmHg). Both, full–empty and filled–empty mode during normal cardiac function led to significantly decreased pulmonary capillary wedge pressure, suggesting load reduction of the right ventricle. In impaired cardiac function, circulatory assistance increased the diminished cardiac output and systolic arterial blood pressure, although only the latter was statistically significant. The authors conclude that the hydraulic pump system is capable of circulatory support in animals similar in size to small infants and that the filled–empty mode with its higher functional flexibility is not inferior to the full–empty mode.

The rotary undulation pump has been developed by a group at the University of Tokyo to meet the demands of long cardiac support. N. Mitsumune et al.[11] from the University of Tokyo investigated fundamental characteristics of a fiber-optic gap sensor toward its application to dynamic position-control of the rotor in the rotary undulation pump. The basic properties of gap sensors using four different light sources [one laser diode (LD) of 785 nm and light-emitting diodes (LEDs) of 644 nm, 700 nm, and 940 nm each) were investigated in five media, such as air, physiologic saline, and blood samples from goats, prepared with three different hematocrits of 20%, 29%, and 40%, respectively. These results demonstrated that fiber-optic gap sensors have a sensing range of approximately 1.3 mm in air, 1.8 mm in physiological saline, and 0.5 mm in blood. The results of measurements in oxygenated blood and deoxygenated blood indicated that the peak positions both in oxygenated blood and in deoxygenated blood were almost the same with the sensor using the 785-nm LD, whereas they were entirely different in the measurements of the sensor using the 644-nm LED. It was also revealed that the sensing range could be adjusted by changing the distance between the emitting fiber and the receiving fiber. Mitsumune and colleagues concluded that the fiber-optic gap sensor is quite promising for the active control of rotor positioning in the rotary undulation pump.

Artificial heart (clinical)

Regarding research papers on clinical applications of the ventricular assist system (VAS), we published one brief communication and two case reports in 2007. T. Komoda et al.[12] reported their implantation technique of the DuraHeart left ventricular assist system (Terumo Heart, Ann Arbor, MI, USA). The authors made some modifications to the implantation technique for the DuraHeart to minimize postoperative bleeding. The DuraHeart is the world's first magnetically levitated centrifugal pump and is expected to be one of the most popular devices in the near future. S. Saito and co-workers[13] reported their experience with the HeartMate vented electric (VE) left ventricular assist system (Thoratec, Pleasanton, CA, USA). They described three cases, all of which were successfully bridged to transplantation. However, the pump stopped in two of the three cases 665 days and 491 days after implantation, and the two patients had to be supported by a backup pneumatic driver thereafter. Their experience showed the problem of long-term durability of the current system. T. Ohata and colleagues[14] reported a simple method of left ventricular assist

system exchange from a BVS-5000 (ABIOMED, Inc. Danvers, MA, USA) to a Toyobo. For longer-term circulatory support, they simply changed from the BVS-5000 to the Toyobo by reconnecting the inflow and outflow lines using appropriate connectors. This technique can be performed outside the body, and an invasive procedure is not necessary. This procedure may be useful in such instances as fulminant myocarditis supported with the BVS-5000.

Cardiopulmonary bypass

In 2007 we published five articles on cardiopulmonary bypass. Two articles were about clinical cardiopulmonary bypass (CPB) circuit and two articles were related to clinical engineering issues. The fifth was a review article on intra-aortic balloon pump (IABP) development.

T. Ohata et al.[15] of the Hyogo College of Medicine evaluated inflammatory reactions in patients in whom a coronary bypass operation was performed with a minimal cardiopulmonary bypass circuit (mini-CPB), a closed system without cardiotomy suction and with an open venous reservoir. They compared IL-6, IL-8, and neutrophil elastase levels of the patients with mini-CPB and conventional CPB (15 patients each). IL-8 levels on postoperative day 1 and neutrophil elastase levels on day 1 and day 2 were significantly lower in the mini-CPB group than in the conventional group. The authors concluded that mini-CPB resulted in lower levels of neutrophil activation and cytokine release after Coronary Artery Bypass Grafting (CABG) than conventional CPB did.

S. Tokunaga et al.[16] of the Kyushu University Hospital reported a case of Extracorporeal Membrane Oxygenation (ECMO) support for a 7-year-old girl weighing 19 kg. She suffered from acute fulminant myocarditis, and the ECMO system was applied because of ventricular tachycardia/ventricular fibrillation (VT/Vf). Seven days after ECMO was started, she was weaned from the ECMO successfully. During ECMO support, Tokunaga and colleagues changed the ECMO flow from 2.0–2.5 l/min to 1.6–1.8 l/min for the decrease of the cardiac afterload. Based on this experience, they suggested that the balance between flow support and LV afterload is important for ECMO management.

Y. Tomizawa and N. Momose[17] of Tokyo Women's Medical University reported the current situation of certified perfusionists in Japan. They reported that 569 certified perfusionists had qualified in Japan up to November 2006, but their geographical distribution is uneven. The authors noted that trained perfusionists are important for the establishment of safe extracorporeal circulation technology.

N. Tsutsui et al.[18] of Tokai Medical Products, Inc. reviewed their development of the IABP balloon catheter and introduced its characteristics. To apply IABP safely and effectively, they conducted scientific studies on the correlation between body height and length of the aorta, suitable balloon diameter, balloon durability, biocompatibility, and other factors. Finally, they produced eight types of IABP balloon catheter. They reduced the catheter shaft diameter from the conventional 8 Fr to 7 Fr. They concluded: "Continuous efforts are being made to provide balloon catheters with many size variations and different specifications, such that optimal balloon catheters can be selected for individual patients with the ultimate aim to provide devices with higher safety and lower invasiveness."

S. Ninomiya et al.[19] of Hiroshima International University reported the development of an educational simulator system for the acquisition of basic perfusion techniques and evaluation. They developed the Extracorporeal Circulation Simulator system (ECCSIM) which simulates a crisis situation during management of a perfusion procedure. Three trials were performed by undergraduate students in clinical engineering. The computer presented instructions for a specific scenario, and the student's performance was recorded. The students were able to learn basic manipulation and experienced perfusionists were able to improve their skills. The authors concluded that the ECCSIM is useful for training perfusionists and provides quantitative feedback on a trainee's performance.

Artificial lung

E. Tatsumi[20] of the National Cardiovascular Center described recent advances in the field of artificial lungs, focusing on the current state and trends in clinical use and on research and development. The author introduced current trends of artificial lung application for ECMO, PCPS, and open heart surgery, and introduced the intracorporeal artificial lung system, all-in-one systems, coating materials, the intravascular oxygenator, respiratory support systems, and computational fluid dynamics (CFD) analysis as representing the current status of research and development. The author concluded that the demand for open heart surgery is stagnating and research and development toward next-generation systems are active, especially in the field of assist circulation. In addition, further expansion of research and development in this field, as well as progress in practical and clinical applications of innovative devices, is expected.

B. Bayrakci et al. [21] of Hacettepe University examined the predictive significance of the oxygen index (OI) as a patient entry criterion for ECMO use. They sought a critical OI level predicting death or chronic lung disease (CLD) with and without ECMO use. Their 6-year experience (1995–2000; 174 patients) showed that an OI of 33.2 is a suitable cutoff value for ECMO initiation with high sensitivity and specificity as a predictive criterion. They concluded that OI is a useful predictor of CLD.

T. Nishinaka et al. [22] of the National Cardiovascular Center applied their new coating material to an ECMO system to realize prolonged cardiopulmonary support with trivial anticoagulant infusion. The circuit tube, cannulae, centrifugal pump, and oxygenator are totally coated with the new material. The system was tested by using a goat model with venoarterial bypass. During 151 days of experiments, they found no significant amounts of thrombus.

Blood vessel prosthesis

In 2007 we had four articles about blood vessel prostheses in the journal: two were about tissue-engineered grafts, one was about a stent graft, and the fourth was about graft infection. T. Watanabe et al. [23] from the Kyoto Prefectural University of Medicine developed a connective tissue tube "biotube" with cuffs at both anastomotic ends. To improve surgical handling of small-diameter thin "biotube" grafts, reinforcement using polyurethane sponge cuffs was applied. An in vivo study was performed in rabbits and the grafts were implanted in the carotid artery position of the same animal. Angiographic evaluation was performed 6 weeks after implantation, and no aneurysmal formation was reported.

Y. Nakayama et al.[24] from the National Cardiovascular Center Research Institute developed autologous connective-tissue-covered metal stents (biocovered stents) in the subcutaneous tissue of rabbits and evaluated burst strength and histological characteristics. The thickness of the covered tissue was less than approximately 200 μm with burst strength of approximately 1000 mmHg. This covered stent with autologous tissue may solve current problems with synthetic polymer-covered stents.

M. Aiba et al.[25] from Showa University, Fujigaoka Hospital, emphasized that to prevent complications after stent graft procedures for treatment of thoracic and thoracoabdominal aortic disease, understanding the anatomical shape of the aorta is important. The relation of gap length and strut direction was studied in an aortic arch model. The authors then manufactured a unibody Z-stent with 10-mm gaps and applied it in seven patients. A minor endoleak developed in one patient, but the result was satisfactory because the frequency of complications decreased.

M. Sacar et al.[26] from Pamukkale University, Turkey, introduced an in vitro model to quantitatively measure bacterial adherence to the surface of a graft. They then determined the role of neuraminidase (NANase) in adherence to gelatin-impregnated polyester fiber fabric graft. They showed the possibility that slime plays an important role in the pathogenesis of vascular graft infection, and adherence of slime-forming *Staphylococcus aureus* could be decreased by NANase treatment.

Artificial valve

In 2007 we published four articles about artificial valves. Three articles reported basic research on mechanical valves or bioprostheses and the other one was on clinical results of bioprostheses.

Formation of cavitation bubbles is still a basic and essential problem in developing a ventricular assist device (VAD). H.S. Lee et al. from the National Cardiovascular Center continued to investigate mechanical heart valve (MHV) cavitation in a VAD. In 2006 they reported formation of cavitation bubbles in an electrohydraulic total artificial heart (EHTAH),[27] and estimation of MHV cavitation in a pneumatic VAD was performed in 2007.[28] Results showed that most cavitation bubbles were observed near the valve stop, and that the cavitation intensity increased as the heart rate increased. The driving pressure slope was found to be related to the valve-closing velocity. They also showed that the cavitation intensity of a pneumatic VAD was less than that for the EHTAH, because the driving pressure slope of the EHTAH was four to five times that of the driving pressure slope of the pneumatic VAD. They concluded that the driving pressure slope in the pneumatic VAD might play a useful role in estimating MHV cavitation intensity.

Numerical analysis of various valve designs provides essential information about the hydrodynamics and the stress of prosthetic heart valves. Y.S. Morsi et al.[29] from the Swinburne University of Technology evaluated a three-dimensional transient numerical approach coupled with fluid–structure interaction for the modeling of an aortic trileaflet heart valve at the initial opening stage. The fluid response was analyzed using an arbitrary Lagrangian-Eulerian formation for analyzing the fluid domain with moving boundaries for the artery structure. Results showed complex stress development patterns during the initial opening of the valve, which was considered to be the most detrimental factor for fatigue failure analysis. It is anticipated that the results from such simulations will provide invaluable information for the design of leaflets of prosthetic heart valves.

It has been reported that analysis of bileaflet mechanical valve sounds may be useful for diagnosis of valve malfunction. H. Sugiki et al.[30] from the Hokkaido University School of Medicine evaluated the properties of various continuous wavelet transforms (CWTs) for analysis of the closing sound of bileaflet mechanical valves in 2006. In 2007 they collected CWT data of five different bileaflet mechanical valves: St. Jude Medical valve, ATS open pivot valve, Carbomedics valve, MIRA valve, and Duromedics valve.[31] Results showed that the split in the bileaflet closing valve sounds is a common finding among the five different types of normally functioning bileaflet valves. They suggested that careful observation of the split behavior of the bileaflet sounds had great potential to detect malfunctions of various kinds of bileaflet mechanical valves.

Although the impact of patient–prosthesis mismatch (PPM) after aortic valve replacement (AVR) remains controversial, it seems clear that PPM may result in high residual transvalvular gradients and has some negative impact on early and late morbidity and mortality. Y. Sakamoto et al.[32] from the Jikei University School of Medicine evaluated valve function and the effects of PPM on midterm results of the 19-mm Carpentier-Edwards Perimount (CEP) pericardial aortic valve in 51 patients aged 65 years or older. The prevalence of PPM was low (17.6%), and the clinical results, postoperative pressure gradients, and reduction in left ventricular mass index were not different between the PPM and no-PPM groups. They concluded that the 19-mm CEP valve provided satisfactory midterm clinical and hemodynamic outcomes in Japanese patients aged 65 years or older.